Numerical modelling of Cr:YAG Q-switched Yb:YAG micro-lasers and comparison with experimental results

Pierre Bourdon, Christophe Planchat, Didier Goular, Laurent Lombard, Francois Gustave, Julien Le Gouët

Numerical modelling of Cr:YAG Q-switched Yb:YAG micro-lasers and comparison with experimental results

P. Bourdon*, C. Planchat, D. Goular, L. Lombard, F. Gustave, J. Le Gouet
ONERA, The French Aerospace Lab, Optics Department (DOTA), BP 80100, 91123 Palaiseau Cedex, France

ABSTRACT

Some applications like range finding, optical counter measures or engine ignition, require lasers capable of delivering high repetition rate bursts of nanosecond pulses with hundreds of microjoules to a few millijoules in terms of energy per pulse.

We previously developed such a diode-pumped Yb:YAG micro-laser with an oscillator delivering 250 µJ to 300 µJ per pulse, with a 3 – 5 ns pulse duration, with an intra-burst pulse repetition frequency that can be tuned continuously from 1 kHz to 20 kHz by increasing the pump power. This oscillator had been amplified to the mJ level by an additional laser module.

But there is a large choice of possible dopant concentration and thickness for the Yb:YAG laser crystal, of low power transmittance value for the Cr:YAG passive Q-switching crystal and of pump power and burst duration, and we want to be sure the choice of design we make is the best one.

In order to optimize this choice of design for the micro-laser, this paper, we developed a numerical model of laser amplification and passive Q-switch. After presenting the model, we describe how it compares with previous results from our own experimental results, in terms of energy per pulse, pulse duration and repetition frequency of the laser and how we managed to obtain good agreement with the experiments by optimizing the numerical modelling of the overlap between the laser and pump beams in the amplifying medium.

Finally, future work to verify the reliability of the numerical model and to use it for optimization of the architecture of the passively Q-switched laser is presented.

Keywords: Solid state laser, passive Q-switch, Yb:YAG, Cr:YAG, high repetition rate, ns pulses, passive cooling

1. INTRODUCTION

Engine ignition is most often triggered by spark plugs, but it can also be done using lasers. One of the most promising technique that is widely studied[1,2] is non-resonant laser breakdown ignition. It is a method that is demanding in terms of laser energy with tens of millijoules per pulse to trigger ignition and even higher energy per pulse for a 100 % probability of ignition.

Multi-pulse laser ignition has been proposed and tested as an option to increase the efficiency of a laser spark plug[3]. Cumulative effects from double pulses have also been observed, optimal pulse spacing being in the order of 100 µs[4]. That's the main application behind the development of high repetition rate Q-switched laser sources that we have done in our team[5,6].

We obtained interesting performances with a diode-pumped Yb:YAG micro-laser in a Master Oscillator Power Amplifier (MOPA) configuration as detailed in Fig. 1.

The laser diodes used for pumping are nLight element© series fiber coupled modules, e3 type for the 40 W DL and e6 type for the 70 W DL. Both are coupled in a 105 µm and 0.22 NA fiber. The 105 µm output of the fiber is magnified into a 210 µm diameter pump beam using a +75 mm collimating achromatic convergent doublet and a +150 mm focusing achromatic convergent doublet from Thorlabs.

*pierre.bourdon@onera.fr; phone (+33)-1-80-38-63-82; fax (+33)-1-80-38-63-45; www.onera.fr

The oscillator is built with a 10 at. % doped 2-mm length Yb:YAG crystal followed by a 85 % initial transmission Cr:YAG crystal and a R = 70 % at 1030 nm concave output coupler with a radius of curvature of 70 mm.

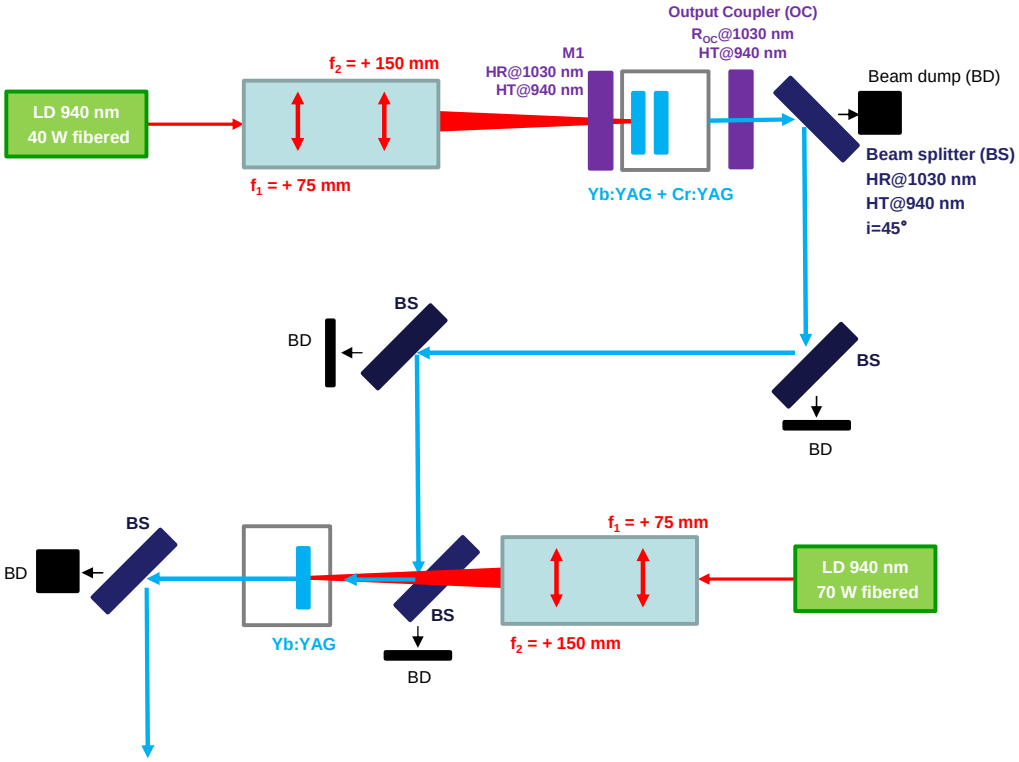

Figure 1. Laser source architecture. A Cr:YAG passively Q-switched Yb:YAG master oscillator (MO) is followed by an Yb:YAG power amplifier (PA) to achieve the expected laser performances.

As we will use this laser as a spark plug, we don't need continuous emission pf the pulses and we chose to operate the oscillator in a "burst emission regime", where 3-ms duration qcw pump pulses repeated at 1 - 5 Hz were used. During these 3 ms of pumping, a burst of short pulses is emitted by the laser with an energy per pulse around 270 µJ, slightly increasing with the pump power level (see Fig. 2, left part). The duration of these pulses is measured between 3 and 4 ns.

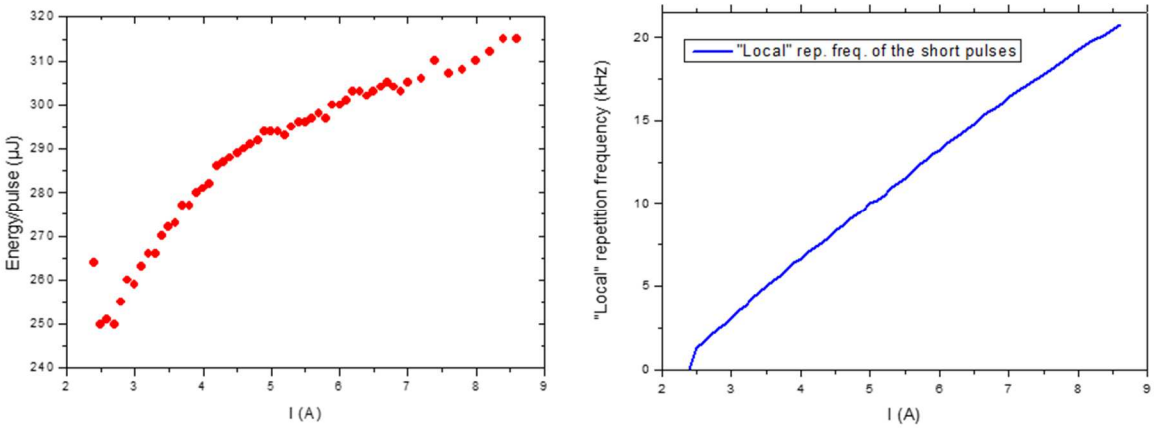

Figure 2. Energy per pulse emitted by the lase oscillator vs. 40-W pump laser diode current (left) and "local" intra-burst repetition frequency of the 4-ns duration pulses as the pump power increases (right).

The repetition rate of the pulses inside a pulse burst increases with pump power from 1 kHz to 20 kHz (see Fig. 2, right part), as can be observed in Fig. 3, resulting in a decrease of the pulse spacing within the bursts. The pulse spacing varies from 50 µs to 1 ms, an optimal range to study the impact of pulse spacing on the multi-pulse laser ignition process.

As the average absorbed pump is between 60 and 300 mW, the advantage of this laser is that it doesn't require active cooling and can operate in a heat-capacity regime with no significant increase of the laser medium temperature during long term laser operation.

If required, it can be amplified in a second Yb:YAG crystal to reach the mJ per pulse energy level.

In the optimization process of the laser oscillator, we compared different Yb:YAG and Cr:YAG crystals, as well as oscillator cavity output couplers (OC). But we never did a complete and exhaustive analysis of the impact of the different characteristics of these components on the performance of the laser oscillator. We want now to design the most effective architecture for this laser oscillator, for both laser ignition tests application and a new application of these laser sources that will require continuous operation of these laser sources that will be used to generate UV light by Third Harmonic Generation in nonlinear crystals.

As we cannot test all the architectures for the laser oscillators, we developed a numerical model capable of predicting the main performances of this laser in order to choose the best components for future realizations. Of course, before using this model for laser source design, we also had to validate its results by comparison with experimental tests. We describe this model and the first results of comparison with experimental tests in the next sections of this paper.

2. NUMERICAL MODELLING OF PASSIVELY Q-SWITCHED YB:YAG LASERS

Numerical models of passively Q-switched Yb:YAG lasers have been developed for a long time now. What we propose here is a synthesis of the main equations we use in the model we chose to develop for our own purpose and a brief presentation of the solver we used.

The numerical model solves the rate equations resulting from two different processes: i) the laser amplification in the Yb:YAG material; ii) the saturable absorption in the Cr:YAG material.

2.1 Numerical model of laser amplification in Yb:YAG

The energy level scheme for the Yb:YAG material is presented in Fig. 3. As Yb:YAG is not a perfect 4-level laser medium but rather a quasi 3-level medium where the lower level of the laser transition can be thermally populated, one has to take into account in the model the impact of the laser medium temperature and the thermal occupancy factors. Fig. 3 gives these occupancy factors at 300 K temperature, which we will consider most of the time as we are developing a very low average power laser where temperature of the laser medium should be very close to ambient temperature.

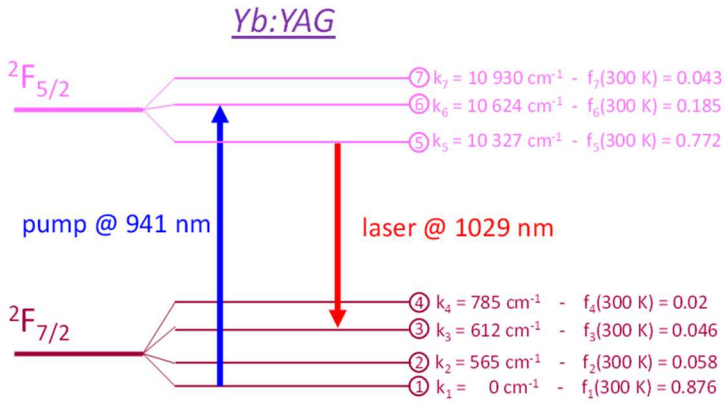

Figure 3. Energy level scheme of Yb:YAG. f_i are the relative thermal occupancies and k_i the wave numbers for the different levels within the two manifolds $^2F_{5/2}$ and $^2F_{7/2}$ involved in the laser process transitions.

Using the same index values as in Fig. 3 to refer to the different energy levels, the relative thermal occupancies[7,8,9] for the different levels involved in the laser process are expressed in the following formulae:

$$f_i = \frac{n_i}{n_L} = \frac{exp\left(-\frac{E_i}{k_B T}\right)}{Z_L} \text{ for } i \in [1\,;4] \text{ and } f_j = \frac{n_j}{n_U} = \frac{exp\left(-\frac{(E_j - E_5)}{k_B T}\right)}{Z_U} \text{ for } j \in [5\,;7] \quad (1)$$

where the n_i values are the population densities for the levels of the lower manifold and the n_j values are the population densities for the levels of the upper manifold, n_L and n_U are the total population densities of lower manifold and upper manifold respectively, $k_B = 1.380649 \cdot 10^{-23}\ m^2\ kg\ s^{-2}\ K^{-1}$ is the Boltzmann constant and T is the temperature in Kelvin.

Z_L and Z_U are the partition functions of lower and upper manifolds respectively and are calculated as:

$$Z_L = \sum_{i=1}^{4} g_i^L exp\left(-\frac{E_i}{k_B T}\right) \text{ and } Z_U = \sum_{i=5}^{7} g_j^U exp\left(-\frac{(E_j - E_5)}{k_B T}\right) \quad (2)$$

For the Yb:YAG material, we have $g_i^L = 1$ for $i \in [1\,;4]$ and $g_j^U = 1$ for $j \in [5\,;7]$. Consequently, we can write equation (2) in a simpler form (2'):

$$Z_L = \sum_{i=1}^{4} exp\left(-\frac{E_i}{k_B T}\right) \text{ and } Z_U = \sum_{i=5}^{7} exp\left(-\frac{(E_j - E_5)}{k_B T}\right) \quad (2')$$

The E_i and E_j values are calculated as: $E_i = hck_i$ and $E_j - E_5 = hc(k_j - k_5)$, with $h = 6.62607015 \cdot 10^{-34}\ m^2\ kg\ s^{-1}$ the Planck constant.

To model laser amplification, we will require some values of the absorption and emission cross-sections of the Yb:YAG medium at the pump wavelength, 941 nm, and the laser wavelength, 1029 nm. More accurately, we will use the average values of these wavelengths corresponding to the central wavelength of the laser spectrum emitted respectively by the laser diode pump and by the Yb:YAG laser itself:

$$\langle\lambda_{pump}\rangle = \frac{10^7}{10624} nm \sim 941{,}2651\ nm \text{ and } \langle\lambda_{laser}\rangle = \frac{10^7}{(10327-612)} nm \sim 1029{,}3361\ nm$$

The values of the absorption and emission cross-sections at these wavelengths can be found in the literature[8]. These values are temperature dependent. We fit the values found in the literature with an exponential decay for increasing temperature. The resulting formulae for the absorption and emission cross-sections of Yb:YAG vs. temperature are the following:

$$\sigma_a(\langle\lambda_{pump}\rangle, T\ in\ °C) = 5.93443 \cdot 10^{-21}\ exp\left(-\frac{T}{216.86934}\right) + 2.81052 \cdot 10^{-21} \quad (3)$$

$$\sigma_e(\langle\lambda_{laser}\rangle, T\ in\ °C) = 1.80901 \cdot 10^{-20}\ exp\left(-\frac{T}{115.99974}\right) + 0.72484 \cdot 10^{-20} \quad (4)$$

The emission cross-section at pump wavelength and absorption cross-section at laser wavelength that we will require for some of the calculations are simply assessed using the well-known McCumber relation:

$$\frac{\sigma_e(\lambda,T)}{\sigma_a(\lambda,T)} = \frac{Z_L}{Z_U}\ exp\left(\frac{\left(E_5 - \frac{hc}{\lambda}\right)}{k_B\ T}\right) \quad (5)$$

For instance, at T = 300 K, using this McCumber relation[10] for Yb:YAG one finds:

$$\sigma_e(\langle\lambda_{pump}\rangle, 300\ K) = 0.212\ \sigma_a(\langle\lambda_{pump}\rangle, 300\ K) \text{ and } \sigma_a(\langle\lambda_{laser}\rangle, 300\ K) = \frac{\sigma_e(\langle\lambda_{laser}\rangle, 300\ K)}{16.6315}.$$

In a real experimental case, using the peak value for the pump absorption cross-section will probably lead to overestimated performances for the laser as this value is too optimistic and does not consider the fact that pumping is done with a 40-W pump laser-diode. As the emission spectrum of this laser diode is quite broad ($\Delta\lambda$ = 5 – 6 nm), the effective absorption cross-section one can assess the effective absorption cross-section at $\langle\lambda_{pump}\rangle$ for the Yb:YAG oscillator we developed from the measurements that were done using our 40-W pump laser-diode. As the emission spectrum of this laser diode is quite large ($\Delta\lambda$ = 5 – 6 nm), the absorption cross section over this spectrum varies significantly and cannot be considered to be the peak value measured at $\langle\lambda_{pump}\rangle$. One has to consider an average value of the cross-section integrated over the broad spectrum of emission of the laser diode.

During the experimental tests, we did measure the effective cross-section corresponding to the average value of the absorption cross-section over its large emission spectrum (see Fig. 4). As this measurement is derived from the

measurement of the fraction of pump power absorbed in the medium, one can consider that it is the effective value of the absorption cross-section to consider when pumping with a broadband laser diode. The effective cross-section value obtained at $\langle\lambda_{pump}\rangle$ is $\sigma_{a,eff}(\langle\lambda_{pump}\rangle, 300\ K) = 7.3837 \cdot 10^{-21}\ cm^2$ instead of the $\sigma_a(\langle\lambda_{pump}\rangle, 300\ K) = 8.22\ 10^{-21}\ cm^2$ value from the literature. This 0.89826 multiplicative factor to assess the effective cross-section when pumping with a broadband laser diode is only to be applied to the cross-sections (absorption and emission) at $\langle\lambda_{pump}\rangle$, as it is due to the broad spectrum emitted by the pump laser. For the assessment of the cross-sections at $\langle\boldsymbol{\lambda_{laser}}\rangle$, as the laser emission spectrum is much narrower, we use the values from the literature.

Another parameter of the model is the radiative lifetime of Yb:YAG which is 951 µs. Due to lifetime-quenching effect, this value measured at 300 K decreases when the temperature of the laser medium increases, but we do not consider this variation in the model.

The rate equations to be solved for numerical modelling of laser amplification in the Yb:YAG laser material are the following ones[11,12,13]:

$$\begin{cases} \dfrac{d\phi}{dt} = \dfrac{\phi}{t_r}\left(2\,\sigma_{em} N\, l - (1 - R_{OC}) - \delta - 2\,\alpha_{las} l\right) \\ \dfrac{dN}{dt} = -2\,\sigma_{em} c \phi N - \dfrac{N}{\tau_{las}} + W_p \end{cases}$$

where ϕ is the photon density in the laser cavity of optical length l_c, N the population inversion density of the laser medium, c is the speed of light in vacuum, $t_r = \frac{2\,l_c}{c}$ is the cavity round-trip time, σ_{em} the emission cross-section at the laser wavelength (1029 nm), l is the length of the Yb:YAG laser gain medium, R_{OC} is the reflectivity of the output coupler mirror and δ are the intracavity dissipative round-trip loss. τ_{las} is the lifetime of the upper laser level, for Yb:YAG, τ_{las} = 951 µs. W_p is the volumetric pump rate.

Some examples of values for these parameters in the case of our experimental demonstration mentioned in the introduction part of this paper: optical cavity length l_c = 5 cm = 0,05 m, l = 2 mm for the 10 at. % doped Yb:YAG crystal, R_{OC} = 70 %. Note that for the reflectivity of the output coupler, as we use some mirrors that are far from high reflectance, we cannot use the low signal approximation of $T_{OC} \approx ln\left(\frac{1}{R_{OC}}\right)$ that would be true for R_{OC} > 90 %.

For the intracavity dissipative round-trip loss, they are induced by the transmission of the R_{max} mirror closing the laser cavity and the loss of the anti-reflection coatings of the crystal faces. Over a round-trip, we pass twice through the 4 crystal faces, each face having a R < 0.2 % coating. Estimating the average reflectivity of these coating to be R_{AR} = 0.15 %, we can assess the loss induced by the 8 passes through these coatings to be close to 1.2 %. We add a 0.5 % loss from the R_{max} = 99.5 % cavity mirror and obtain δ = 0.0017 = 1.7 %.

Both for pump absorption and laser absorption in the Yb:YAG crystal, we can use the absorption coefficient $\alpha = \sigma\,[Yb^{3+}]$ where $[Yb^{3+}]$ is the doping density. For a 1 % at. doped Yb:YAG crystal[13], $[Yb^{3+}] = 1.38 \cdot 10^{20}\ cm^{-3}$. Consequently, for our 10 % at. doped Yb:YAG crystal, we have $[Yb^{3+}] = 1.38 \cdot 10^{21}\ cm^{-3}$.

We can apply this formula to calculate $\alpha_{las} = \sigma_a(\langle\lambda_{laser}\rangle, T)\,[Yb^{3+}]$. We can also use it to calculate the pump absorption coefficient $\alpha_{pump} = \sigma_a\left(\langle\lambda_{pump}\rangle, T\right)[Yb^{3+}]$. This coefficient is helpful in assessing the volumetric pump rate:

$$W_p = \frac{P_{pump}\left(1 - exp\left(-\alpha_{pump} l\right)\right)}{h\,\upsilon_{pump}\,A_{pump}\,l}$$

where P_{pump} is the average pump power and A_{pump} the area of the pump beam that can be calculated from the 1/e radius of for a gaussian beam as this 1/e radius is the radius of an equivalent uniform laser beam (top-hat) comprised of the same overall energy. For instance, in our experimental configuration, the pump beam has a 1/e² diameter of 210 µm and we calculate A_{pump} from the 1/e diameter which is 148.5 µm.

We will assume in the numerical model that the laser amplification occurs transversally within this area A_{pump}, that will be used to assess the photon density ϕ as well as the population densities.

Spontaneous emission is necessary to start the emission process as the first rate equation is proportional to ϕ. Without spontaneous emission, ϕ will remain null while running the numerical model. We use a simple assessment of the spontaneous emission factor by assuming that only the light emitted within the solid angle of the laser pumped area inside the cavity contributes to seeding the laser emission. We define S, the spontaneous emission factor corresponding to the fraction of spontaneous emission contributing to the lasing process within the cavity by the formula:

$$S = \frac{A_{pump}}{4\,\pi\,l_c^2}$$

Spontaneous emission is added to the first rate equation by an additional $\frac{SN}{\tau_{las}}$ term.

We also have to consider the fact that the lower levels of both manifolds are partially thermally depleted and consider the impact of the relative thermal occupancies f_5, f_3 and f_1 on the rate equations. f_1 is somehow already considered in the pump absorption coefficient. In fact, the effective cross-section calculated previously and formerly explained by the large bandwidth of the laser diode used here can also be attributed to the f_1 factor. In fact, it's quite exactly equal to f_1 at 300 K.

The effective cross-section multiplicative factor is probably a mix between the impact of f_1 and of the pump laser broadband and such a factor of 0.87 to 0.89 should be used in any case. As the pumping only lasts for a few microseconds, there's not enough time for the laser medium to thermalize and we don't have to apply the f_5 factor, we can consider that the pump process only populates the upper state level of the laser transition (level 5 in Fig. 3). If we had operated in a continuous-wave regime, we would have to apply the f_5 multiplicative factor to the *Wp* term in the second equation to obtain the effective population inversion *N*.

Finally, the f_3 factor leads to a non-zero population of the lower level of the laser transition that will be taken into account by defining N as $N = N_5 - N_3 = N_5 - f_3[Yb^{3+}]$.

The final rate equations system is:

$$\begin{cases} \dfrac{d\phi}{dt} = \dfrac{\phi}{t_r}\left(2\,\sigma_{em}(N_5 - f_3[Yb^{3+}])\,l - (1 - R_{OC}) - \delta - 2\,\alpha_{las}l\right) + \dfrac{S(N_5 - f_3[Yb^{3+}])}{\tau_{las}} \\ \dfrac{dN_5}{dt} = -2\,\sigma_{em}c\phi(N_5 - f_3[Yb^{3+}]) - \dfrac{(N_5 - f_3[Yb^{3+}])}{\tau_{las}} + W_p \end{cases}$$

2.2 Numerical model of saturable absorption in Cr:YAG

Next step is to add the passive Q-switch operated by the Cr:YAG crystal to the numerical model. Cr:YAG passive Q-switching has been studied in the past. To obtain a realistic formula for the passive Q-switch, one has to consider not only the saturable absorption effect from the ground state of theCr:YAG material, but also the absorption from an excited state of the material.

There are consequently two additional rate equations to solve when the Cr:YAG crystal is added inside the laser cavity[12]:

$$\begin{cases} \dfrac{dN_{gs}}{dt} = -2\,\sigma_{gs}c\phi N_{gs} + \dfrac{N_{sa0} - N_{gs}}{\tau_{es}} \\ N_{es} = N_{sa0} - N_{gs} \end{cases}$$

The rate equation for the photon density has also to be modified adding two terms:

$$\frac{\phi}{t_r}\left(-2\,\sigma_{gs}N_{gs}l_{sa} - 2\,\sigma_{es}N_{es}l_{sa}\right)$$

In these equations, σ_{gs} and σ_{es} are the absorption cross-sections of ground state and excited state of the saturable absorber, respectively, l_{sa} is the length of the saturable absorber and N_{gs} and N_{es} are the ground state and excited state population densities of the saturable absorber respectively. N_{sa0} is the total population density of the saturable absorber and τ_{es} the lifetime of the excited state of the saturable absorber.

The absorption cross-sections and lifetime of excited state for Cr:YAG are now well known even if the measurement of the cross-sections were not obvious and took some time to converge toward reliable values.

We use the most recent and reliable ones[11]: $\sigma_{gs} = 4.6 \cdot 10^{-18}\ cm^2$, $\sigma_{es} = 8.2 \cdot 10^{-19}\ cm^2$ and $\tau_{es} = 3.4\ \mu s$.

To assess N_{sa0}, one needs to measure the length of the Cr:YAG crystal, $l_{sa} = 1.6\ mm$ in our experimental configuration, and to know the initial transmission of the crystal $T_0 = 85\ \%$ in our experimental configuration. As $T_0 = exp(-\sigma_{gs} l_{sa} N_{sa0})$, it's easy to assess: $N_{sa0} = \frac{-ln(T_0)}{\sigma_{gs} l_{sa}}$.

It's also possible to assess the maximum transmission of the saturable absorber that is reached once the absorber has completely bleached: $T_{max} = exp(-\sigma_{es} l_{sa} N_{sa0}) = T_0^{\frac{\sigma_{es}}{\sigma_{gs}}}$.

2.3 Complete numerical model of Cr:YAG passively Q-switched Yb:YAG laser

Combining the rate equations from sections 2.1 and 2.2, we obtain this final set of 4 rate equations that we will solve using an adaptive step Runge-Kutta algorithm.

$$\begin{cases} \frac{d\phi}{dt} = \frac{\phi}{t_r}\left(2\,\sigma_{em}(N_5 - f_3[Yb^{3+}])\,l - 2\,\sigma_{gs}N_{gs}l_{sa} - 2\,\sigma_{es}N_{es}l_{sa} - (1 - R_{OC}) - \delta - 2\,\alpha_{las}l\right) + \frac{S(N_5 - f_3[Yb^{3+}])}{\tau_{las}} \\ \frac{dN_5}{dt} = -2\,\sigma_{em}c\phi(N_5 - f_3[Yb^{3+}]) - \frac{(N_5 - f_3[Yb^{3+}])}{\tau_{las}} + W_p \\ \frac{dN_{gs}}{dt} = -2\,\sigma_{gs}c\phi N_{gs} + \frac{N_{sa0} - N_{gs}}{\tau_{es}} \\ N_{es} = N_{sa0} - N_{gs} \end{cases}$$

To test the equations and the validity of the model, we started by using a very simple and fast Runge-Kutta first order algorithm with a relative tolerance of 10^{-2}.

In the future, we will implement more accurate Runge-Kutta algorithms like fourth order Runge-Kutta. Conversion to Python IDE is also ongoing.

3. NUMERICAL RESULTS AND CONCLUSION

Using the numerical model described in details in section 2, we were able to reproduce quite accurately the results from our experimental configuration, both in terms of pulse repetition frequency and pulse duration, even with a RK 1 solver that doesn't offer the best accuracy we can expect. The adaptive step process allows for fast computation time of only 10 to 15 s.

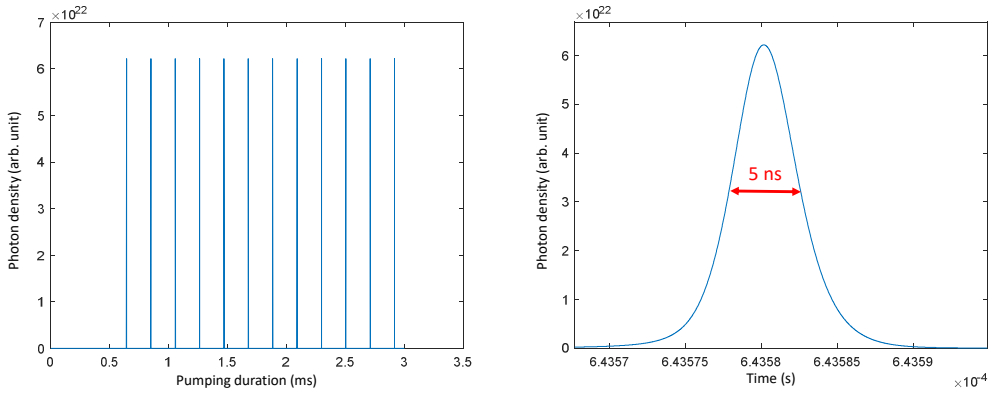

Figure 4. Example of numerically modelled pulse burst at 4.8 kHz "local" repetition rate (left) and zoom on one of the pulses of the burst. This repetition frequency of 4.8 kHz is a little lower than the 6.6 kHz frequency observed when operating with a 10-W level of emitted pump power, that served as an input value for the model.

Fig. 4 presents an example of pulse burst and pulse profile at a repetition frequency of 4.8 kHz. The level of pump power introduced in the numerical model is 10 W. For this level of emitted pump power, we experimentally observed higher repetition rates close to 7 kHz. The energy per pulse obtained with the model is 350 µJ and is higher than the 270 µJ measured experimentally.

The 5-ns pulse duration from the numerical model perfectly fits the value measured experimentally.

We tried to change the input parameters of the numerical model and it appeared that we could fit both the 7 kHz repetition rate and the 270 µJ energy per pulse just by changing the value for the pump beam diameter. This value defines the area in which the laser amplification process occurs. Decreasing the 210 µm value for the $1/e^2$ laser beam diameter to 185 µm, we observed excellent agreement between the simulated and measured values for the repetition rate and the pulse energy.

We now want to go further into the comparison with our experimental data, and to explore in more details this comparison by trying to compare results from different publications with our model's.

Once the model demonstrated as reliable, future work will use it to optimize the design of the laser oscillator and choose the best crystals, both Yb:YAG and Cr:YAG, as well as the best output couplers for the laser performance.

REFERENCES

[1] Bradley, D., Sheppard, C. G. W., Suardjaja, I. M. and Woolley, R., "Fundamentals of high-energy spark ignition with lasers," Combustion and Flame 138(1-2), 55-77 (2004).

[2] Phuoc, T. X., "Laser-induced spark ignition fundamentals and applications," Optics and Lasers in Engineering 44(5), 351-397 (2006).

[3] Tsunekane, M., Inohara, T., Ando, A., Kido, N., Kanehara, K. and Taira, T., "High peak power, passively Q-switched microlaser for ignition of engines," IEEE Journal of Quantum Electronics, 46(2), 277-284 (2010).

[4] Bak, M. S., Im, S., and Capelli, M. A., "Successive laser-induced breakdowns in atmospheric pressure air and premixed ethane-air mixtures," Combustion and Flame 161(7), 1744-1751 (2014).

[5] Bourdon, P., Planchat, C., Fleury, D., Le Gouët, J., Gustave, F., Dolfi-Bouteyre, A., Lombard, L., Jacqmin, H. and Durécu, A., "Passively Q-switched Yb:YAG micro-laser for high peak power high repetition rate burst of pulses emission," Proc. SPIE 10896, 108960J (2018).

[6] Bourdon, P., Planchat, C., Fleury, D., Le Gouët, J., Gustave, F., Dolfi-Bouteyre, A., Lombard, L., Durécu, A. and Jacqmin, H., "Passively cooled Cr:YAG Q-switched Yb:YAG micro-laser delivering continuously tunable high repetition rate bursts of short pulses," Proc. SPIE 10896, 108960J (2019).

[7] Brown, D. C., Tomasello N. S. and Hancock, C., "Absorption and emission cross-sections, Stark energy levels, and temperature dependent gain of Yb:QX phosphate glass," Opt. Express 29 (21), 33818-33835 (2021).

[8] Koerner, J., Vorholt, C., Liebetrau, A., Kable, M., Kloepfel, D., Seifert, R., Hein, J. and Kaluza, M. C., "Measurement of temperature-dependent absorption and emission spectra of Yb:YAG, Yb:LuAG, and Yb:CaF_2 between 20°C and 200°C and predictions on their influence on laser performance," J. Opt. Soc. Am. B. 29 (9), 2493-2502 (2012).

[9] Ostermeyer, M. and Straesser, A., "Theoretical investigation of feasibility of Yb:YAG as laser material for nanosecond pulse emission with large energies in the Joule range," Opt. Comm.. 274, 422-428 (2007).

[10] McCumber, D. E., "Einstein relations connecting broadband emission and absorption spectra," Phys. Rev. 136 (4A), 954-957 (1964).

[11] Dong, J. , Shirakawa, A. and Ueda, K-I., "Numerical simulation of a diode-laser-pumped self-Q-switched Cr,Yb:YAG microchip laser," Opt. Rev. 12 (3), 170-178 (2005).

[12] Ma, J., Dong, J., Ueda, K-I. and Kaminskii, A.A., "Optimization of Yb:YAG/Cr^{4+}:YAG composite ceramics passively Q-switched microchip lasers," Appl. Phys. B 105 (4), 749-760 (2011).

[13] Koechner, W., [Solid-State Laser Engineering], Springer Science+Business Media, New-York, (2006).